Identification of Subsurface Oxygen Species Created during Oxidation of Ru(0001)

Raoul Blume,*,† Horst Niehus,† Horst Conrad,‡ Artur Böttcher,# Lucia Aballe,§ Luca Gregoratti,§ Alexei Barinov,§ and Maya Kiskinova*,§

Institut für Physik der Humboldt-Universität, Newtonstrasse 15, 12489 Berlin, Germany, Fritz-Haber-Institut der Max-Planck-Gesellschaft, Faradayweg 4-6, 14195 Berlin, Germany, Institut für Physikalische Chemie, Universität Karlsruhe, Kaiserstrasse 12, 76131 Karlsruhe, Germany, and Sincrotrone Trieste, AREA Science Park-Basovizza, Trieste-34012, Italy

Received: December 22, 2004; In Final Form: February 28, 2005

The oxidation states formed during low-temperature oxidation ($T < 500$ K) of a Ru(0001) surface are identified with photoelectron spectromicroscopy and thermal desorption (TD) spectroscopy. Adsorption and consecutive incorporation of oxygen are studied following the distinct chemical shifts of the Ru $3d_{5/2}$ core levels of the two topmost Ru layers. The evolution of the Ru $3d_{5/2}$ spectra with oxygen exposure at 475 K and the corresponding O_2 desorption spectra reveal that about 2 ML of oxygen incorporate into the subsurface region, residing between the first and second Ru layer. Our results suggest that the subsurface oxygen binds to the first and second layer Ru atoms, yielding a metastable surface "oxide", which represents the oxidation state of an atomically well ordered Ru(0001) surface under low-temperature oxidation conditions. Accumulation of more than 3 ML of oxygen is possible via defect-promoted penetration below the second layer when the initial Ru(0001) surface is disordered. Despite its higher capacity for oxygen accumulation, also the disordered Ru surface does not show features characteristic for the crystalline RuO_2 islands. Development of lateral heterogeneity in the oxygen concentration is evidenced by the Ru $3d_{5/2}$ images and microspot spectra after the onset of oxygen incorporation, which becomes very pronounced when the oxidation is carried out at $T >$ 550 K. This is attributed to facilitated O incorporation and oxide nucleation in microregions with a high density of defects.

1. Introduction

An important step in the oxidation of transition metal surfaces is the accumulation of oxygen in subsurface sites during the transition from an adsorption to a stable oxide phase. Theoretical studies of the initial oxidation process have suggested that after saturation of the adsorption phase, the next important intermediate step is the incorporation of O atoms between the first and second atomic layer of the transition metal (TM), followed by the formation of a trilayer O-TM-O structure, called surface oxide.[1,2] Despite the enormous experimental efforts aimed at providing evidence for subsurface oxygen species the assignment of spectroscopic features to subsurface oxygen still remains ambiguous. A great part of these efforts have been focused on Ru, a technologically important catalyst that exhibits different catalytic properties at low and high oxygen pressures, attributed to the necessity to form the active rutile RuO_2 catalyst phase.[3−9] The chemical state and the morphology of the Ru(0001) surface after exposure to O_2 under different conditions have been intensively investigated at atomic, mesoscopic, and macroscopic levels, applying a great variety of structural and spectroscopic techniques.[4,5,8−13] The capacity of Ru for accumulation of oxygen is remarkably high. The Ru−O bonding configuration, which determines the oxidation state, depends strongly on the oxidation conditions (O_2 pressure, sample temperature, O_2 dose, and morphology of the surface).[8−11] For high oxygen pressures the amount of accumulated oxygen and the Ru oxidation state are controlled by the sample temperature. Most studies are carried out at temperatures higher than 600 K, when large RuO_2-(110) domains are formed after high oxygen doses.[4−6,12] Using XPS microscopy we demonstrated that the spatial anisotropy of the oxide growth, first evidenced with PEEM,[10] is due to coexisting adsorption and intermediate O-rich states preceding the nucleation and growth of rutile RuO_2(110) islands.[12] However, many open questions remain concerning the transition from adsorption to complete oxidation and formation of stoichiometric RuO_2(110). In particular, the states formed at lower temperatures are relevant to understanding the reactivity behavior under different reaction conditions.

Employing thermal desorption spectroscopy (TDS), low-energy electron diffraction (LEED), thermal energy atom scattering (TEAS), and ultraviolet photoelectron spectroscopy (UPS), we have already shown that the oxygen incorporation into the subsurface region does not yield a crystalline bulk RuO_2-(110) phase at temperatures lower than 550 K for O_2 pressure up to 1 bar.[14] In the present TDS-XPS microscopy study we identify the oxidation states formed at low temperature (LT), which differ from the crystalline rutile RuO_2 formed under high temperature (HT) oxidation. Using a spatially resolved chemically sensitive technique, the spatial anisotropy during the oxidation process is followed and the role of defects in the different stages of Ru oxidation is investigated. Combining the LT and HT results we present a diagram, which describes the oxidation state of the Ru(0001) surface as a function of the

* Corresponding authors. E-mail: raoul.blume@physik.hu-berlin.de and maya.kiskinova@elettra.trieste.it. URL: http://asp2.physik.hu-berlin.de and http://www.elettra.trieste.it.

† Institut für Physik der Humboldt-Universität.

‡ Fritz-Haber-Institut der Max-Planck-Gesellschaft.

Universität Karlsruhe.

§ Sincrotrone Trieste.

10.1021/jp044175x CCC: $30.25
Published on Web 07/06/2005

sample temperature and O_2 exposure. This diagram clearly defines the boundaries in the (Exposure, *T*)-space where the growth of bulk RuO_2 is kinetically hindered and only incorporated oxygen or a metastable "surface oxide" exists.

2. Experimental Section

The XPS microscopy experiments were carried out with the scanning photoemission microscope (SPEM) operating at the ESCA microscopy beamline at Elettra. The SPEM uses a zone plate as photon focusing optic and a hemispherical electron energy analyzer with a 48 channel detector. A detailed description of the beamline, UHV preparation chambers, and the SPEM can be found in ref 15. The measurements were performed with photon energies of 504 and 450 eV, an energy resolution of 0.18 eV, and a lateral resolution of 150 nm. By using the universal curve for the electron mean free path[16] the effective escape depth for Ru 3d photoelectrons in our grazing geometry is estimated to be ~3.8 Å at 450 eV. It should be noted that the high surface sensitivity of our measurements limits the useful information depth exclusively to the two topmost layers and the average information volume is of the order of 1000 nm^3. The scanning and sample positioning system allows two different operating modes: imaging and microspot XPS. Imaging is performed by synchronously scanning the sample and collecting the emitted photoelectrons. The images, after removal of the background contribution, reflect variations in the concentration and chemical state of the chosen element. The 48-channel detector allows mapping of different chemical states, removal of the topography and background contributions, as well as reconstruction of the spectrum corresponding to the selected energy window used for imaging (spectroimaging). Spectroimaging is extremely useful for monitoring dynamic "chemical" processes and controlling possible photon-induced effects. The latter are time dependent and for some intermediate Ru oxidation states visible changes due to oxygen reduction were observed in the spectra for acquisition times longer than 20 s. With use of the spectroimaging mode, where the illumination time is <1 s/pixel, the photon-induced effects on the O−Ru states were negligible.

A clean, well-ordered Ru(0001) surface is obtained by cycles of Ar^+ sputtering and subsequent annealing in O_2 ambient, as described in ref 17. The role of surface defects in the accumulation of oxygen is investigated by generation of surface roughness, gently sputtering the smooth surface. This led to creation of defects with lateral density of ~0.8 ML.[14]

The oxidation was carried out in a high-pressure chamber connected to the microscope UHV chamber. The sample temperature was controlled with a K-type thermocouple spot-welded to the backside of the sample. The amount of accumulated oxygen was determined by using as a reference the integral of the O_2 TD spectra corresponding to a completed chemisorbed monolayer ($1\ ML = 1.58 \times 10^{15}\ cm^{-2}$), showing a (1×1)- LEED pattern.[18] All TD spectra were obtained with a constant heating rate of 4 K/s.

The $Ru3d_{5/2}$ spectra were fitted by using asymmetric Doniach-Sunjic functions convoluted with Gaussian profiles, following the strategy described in ref 19. The accuracy of the peak positions for different fits is better than 0.05 eV. For the deconvolution of the spectra from the disordered phases with not well-defined multiple coordination possibilities, broadening of the components was allowed.

3. Results

The development of the different states during Ru(0001) oxidation was followed by monitoring the Ru $3d_{5/2}$ core level spectra, which are very sensitive to the O environment. In contrast, the O 1s core level spectra are rather broad without distinct features of the different states and cannot be used for unambiguous discrimination of the intermediate oxidation states.[12,13] The top three cells of Table 1 summarize the energy positions of the Ru $3d_{5/2}$ components corresponding to the clean surface, the adsorption phases, and the RuO_2 phase, already measured with high-resolution XPS and supported by theoretical calculations.[12,13,19] The Ru $3d_{5/2}$ spectrum of the clean Ru(0001) contains the following three components: a "bulk" component, reflecting the emission from the Ru atoms below the second layer, a surface component originating from the top Ru layer, Ru(I), and the second Ru layer component, Ru(II).[19] In all plots with Ru $3d_{5/2}$ spectra we used as a zero-energy reference the position of the Ru(b), 280.1 eV. At lower oxygen exposures only the Ru(I) component undergoes chemical shifts, determined by the number of adsorbed oxygen atoms bonded to the first layer Ru atoms, which increases from 1 to 3. That is why, for fitting the spectra from the adsorption phases, for simplicity one can use one broader component to account for the "bulk" and Ru(II) contributions.[19] The rutile $RuO_2(110)$ phase is characterized by two components corresponding to 5-fold coordinated Ru atoms at the RuO_2 surface, Ru-cus, and 6-fold coordinated Ru atoms in the bulk, RuO_2.[13,20] Another distinct feature of the RuO_2 phase is a broad satellite at ≈282.7 eV between the Ru $3d_{3/2}$ and $3d_{5/2}$ peaks.[12] This satellite grows with the formation of an ordered RuO_2 and is visible already for three rutile layers.

TABLE 1: Binding Energy Shifts with Respect to the Ru $3d_{5/2}$ Bulk Peak (280.1 eV) of the Components Corresponding to the Differently O-Coordinated Atoms from the First Ru(I) and Second Ru(II) Layers and of the Bulk and Surface Ru-cus Atoms of the Crystalline $RuO_2(110)$

binding energy (eV)	spectral feature	ref
0	bulk	
−0.35	R(I)	19
0.15	Ru(II)	19
0.02	Ru(I)−1O	19
0.39	Ru(I)−2O	19
0.93	Ru(I)−3O	13, 19
0.65	RuO_2	12, 13
0.35	Ru-cus	13
2.6	satellite	12
0.4	Ru_xO_y	
0.5	Ru(II)−O	
1.4	Ru(I)−4O	
0.8−0.85	Ru(I)−4O*	

A. Oxidation of an Ordered Ru(0001) Surface. For the sake of comparison we will start with an introductory figure, which illustrates the difference in the Ru $3d_{5/2}$ images and spectra of advanced HT and LT states. Figure 1 shows Ru $3d_{5/2}$ images and the corresponding Ru $3d_{5/2}$ spectra of clean Ru(0001) (a) and Ru(0001) exposed to high O_2 doses at different sample temperatures, representing an advanced HT (b) and "O-saturated" LT (c) oxidation states. The deconvolution of the Ru $3d_{5/2}$ spectra is performed by using the already known $3d_{5/2}$ core level shifts and some new components, the origin of which is established in the present study and reported in the bottom block of Table 1.

The Ru $3d_{5/2}$ image of the clean Ru (a) contains only topographic features due to scratches, introduced during polishing. These topographic features were avoided in micro-XPS measurements but served as markers to find the same surface area during the LT oxidation cycles, when the sample was transferred between the microscope and the high-pressure cell. The Ru $3d_{5/2}$ spectrum taken away from the topographic features

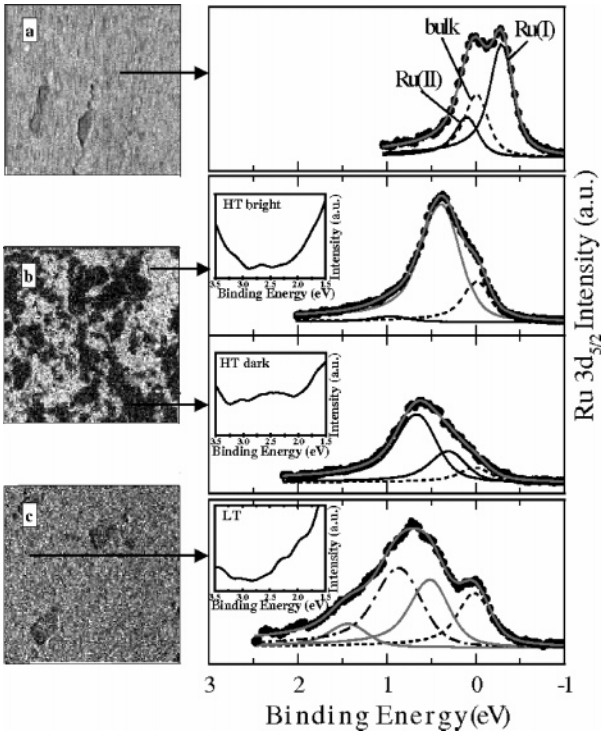

Figure 1. Left panel: $64 \times 64\ \mu m^2$ Ru $3d_{5/2}$ images of (a) the clean surface and after (b) HT ($P_{O_2} = 5 \times 10^{-3}$ mbar, $T = 775$ K, 7.5×10^4 mbar s) and (c) LT ($P_{O_2} = 1$ bar, $T = 475$ K, 10^{12} mbar s) oxidation procedures. Right panel (top to bottom): Ru $3d_{5/2}$ spectra taken from the areas of the Ru $3d_{5/2}$ images, indicated by the arrows. The Ru $3d_{5/2}$ spectra are deconvoluted according to the procedure described in the text, using the components shown in Table 1. The dotted line is the Ru $3d_{5/2}$ bulk component. The insets show the energy range of the satellite peak, which is present only in the spectra from the dark areas of the HT oxidation state.

can be fitted by using the "bulk", Ru(II), and Ru(I) components reported in Table 1.[19] The Ru(I) component is considerably reduced and poorly resolved in the Ru$3d_{5/2}$ spectra from defect-rich areas. The Ru $3d_{5/2}$ image of the advanced HT oxidation state (b) is completely different. It consists of dark and bright regions, which result from significant variations in the total Ru $3d_{5/2}$ intensity, not related to surface topography. Since the RuO_2 phase contains fewer Ru atoms per unit volume than the adsorption and intermediate O-rich states,[2] it should appear the darkest in the Ru $3d_{5/2}$ images. The assignment of the dark regions to rutile RuO_2 islands is confirmed by the corresponding Ru $3d_{5/2}$ spectra, consisting of RuO_2 and Ru-cus components. Because of the limited escape depth of the Ru $3d_{5/2}$ photoelectrons the "bulk" component is practically absent, indicating that the oxide thickness has exceeded 3 rutile layers.[12] Another distinct fingerprint of the RuO_2 islands is the "oxide" satellite feature growing on the left side of the Ru $3d_{5/2}$ spectrum. The Ru $3d_{5/2}$ spectrum from the bright regions is very different. It still contains a "bulk" component and two more components. The spectrum presented here is dominated by a component at $\sim$0.4 eV. The assignment of this component to an adsorption state should be ruled out, because of the strong attenuation of the "bulk" component, indicating growth of $\sim$6 Å film with incorporated oxygen, comparable with the thickness of two O−Ru−O trilayers.[21] Since the energy position of this component is comparable with that of the unsaturated cus-Ru atoms, we tentatively assign it to multiple O-coordinated Ru, Ru_xO_y, in intermediate amorphous O-rich states limited to the top few layers. The best fit also requires another weak component at $\sim$0.85 eV, the origin of which is related to an earlier oxidation state, discussed below. The assignment of the bright areas to an intermediate amorphous oxidation state is further supported by the absence of an "oxide" satellite feature.[12]

The Ru $3d_{5/2}$ image of the "oxygen-saturated" LT oxidation state appears homogeneous at this rather large length scale, excluding the visible topographic features, as those on the clean surface. The Ru $3d_{5/2}$ spectra of this state differ from that of the RuO_2 domains: they are very broad, centered at $\sim$0.75 eV, with a strong contribution of components at higher binding energies and no satellite feature. The intensity of the "bulk" component is strongly reduced. This indicates high content of incorporated oxygen in various bonding configurations, requiring more fitting components, the origin of which is described below.

The TD spectra taken after the same HT and LT preparation cycles provided the quantitative information about the amount of accumulated oxygen, which cannot be obtained by the photoemission spectra, because of the limited probing depth. Indeed, the O_2 TD spectra cannot account for the spatial anisotropy of the HT "oxidized" Ru but their integral intensities confirmed the very different total O content for the advanced HT and LT oxidation states in Figure 1, $\sim$7 and 3 ML, respectively.

To identify the origin of the components required for deconvolution of the Ru $3d_{5/2}$ spectra of the LT oxidation state we followed in detail their evolution while increasing the oxygen dose at 475 K. The system first passes through several ordered adsorption states until the maximum oxygen coverage of 1 ML is attained.[19,20,22] The upper pair of Ru $3d_{5/2}$ spectra in Figure 2 are taken after an exposure necessary to achieve a saturated (1×1) adsorption state. They are measured in two different microspots and have somewhat different line shapes, reflecting the spatial heterogeneity that develops close to the saturation of the adlayer, when oxygen starts to incorporate. In both spectra the component at $\sim$0.9 eV corresponding to Ru(I)−3O in the saturated (1×1) adsorption phase is present. The top spectrum represents an unsaturated (1×1) adsorption phase, where there are still hcp oxygen vacancies: the component at $\sim$0.4 eV corresponds to Ru(I)−2O. The second spectrum shows a more advanced state, most likely from regions with higher density of defects or irregularities at atomic and nanoscopic scale, which facilitate oxygen incorporation.[14] Such regions might also lead to the observed anisotropy in the oxide growth in the advanced HT oxidation states (see Figure 1b). In the second spectrum the intensity of the Ru(I)−3O component has increased, indicating that the (1×1) adsorption phase in this region has saturated. In addition a weak but distinct component at about 0.5 eV has appeared that does not belong to any of the oxygen adsorption phases. This new feature belongs to the next state with oxygen incorporated between the first and second Ru layers. The presence of incorporated O atoms is detected as the emerging α-peak at 1040 K in the corresponding TD spectra, shown in the right panel. The α-peak appears only when the oxygen coverage exceeds 1 ML, i.e., when along with the saturated (1×1) adsorption phase some oxygen has already penetrated between the first and second Ru layers.[11]

The assignment of the $\sim$0.5 eV feature to subsurface oxygen is supported by the evolution of the Ru $3d_{5/2}$ spectra with increasing O_2 dose. The third Ru $3d_{5/2}$ spectrum ($\sim$1.5 ML) in Figure 2 is obtained after considerably higher oxygen exposure of 10^8 mbar·s. Here, the 0.5 eV component has gained intensity and another two components peaked at $\sim$0.8 and $\sim$1.4 eV give the best fit. The recent DFT calculations predict that with increasing oxygen content in the subsurface region the first layer Ru atoms can bind to 4 oxygen atoms, the fourth oxygen being

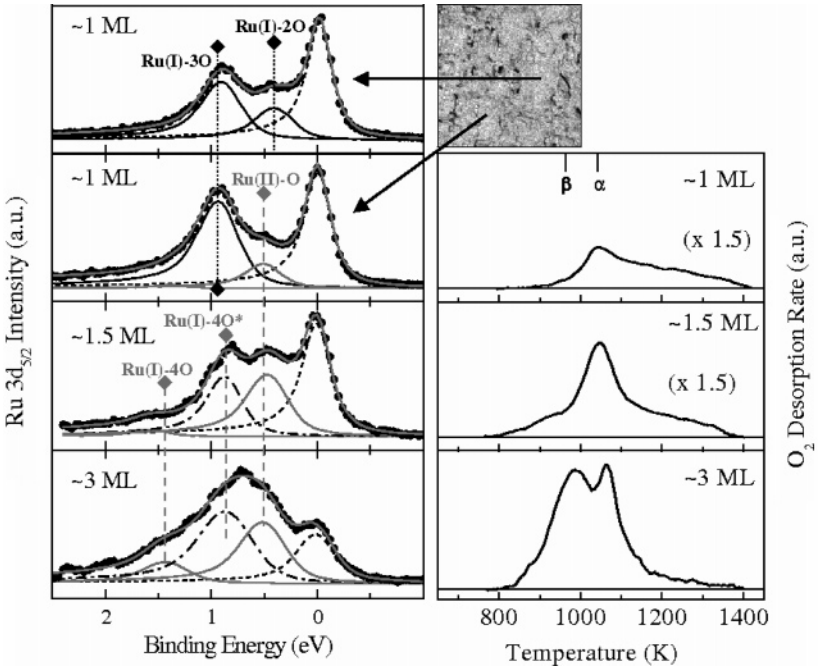

Figure 2. Left panel: (top to bottom) Ru $3d_{5/2}$ spectra taken after exposure of an ordered Ru(0001) surface at 475 K to 10^5 (~1 ML), 10^8 (~1.5 ML), and 10^{12} mbar s (~3 ML). The top two spectra are taken in different regions of the corresponding Ru $3d_{5/2}$ image, indicated by the arrows. The deconvolution is performed with use of the components shown in Table 1. The assignment and the positions of the different components are indicated by vertical lines in the plot. The dotted line is the Ru $3d_{5/2}$ bulk component. Right panel: The TD spectra, which quantify the oxygen content of the corresponding Ru $3d_{5/2}$ spectra in the left panel to ~1, ~1.5, and ~3 ML, respectively.

located beneath the first layer.[1,2,21] It is suggested that the accumulation starts in the form of small islands followed by an expansion of the lattice. The component at ~0.5 we tentatively ascribe to the a shift of the Ru(II) component, induced by binding of the Ru atoms from the second layer to the incorporated O (Ru(II)−O in Table 1). It is plausible to assume that the incorporated O, O_{sub}, will also affect the binding energy of the top Ru(I)−3O atoms. The O_{ad}−Ru(I)−O_{sub} bonding configuration should depend on the interstitial (tetra- or octa-) sites where the O is located. We tentatively assign the components at ~0.8 and 1.4 eV to two different O_{ad}−Ru(I)−O_{sub} states with O in tetra- and octahedral sites, respectively. It should be noted that the component Ru(I)−4O at ~1.4 eV obeys the linear behavior of the binding energy shifts of the surface Ru atoms with increasing oxygen coordination.[23,24] Another plausible assignment of the Ru(I)−4O components at ~0.8 eV and ~1.4 eV is that they reflect the additional core level shift undergone by the Ru(I) atoms bonded to 2 or 3 O adatoms, induced by the oxygen atoms incorporated below. This leads to configurations Ru(I)−$2O_{ad}O_{sub}$ and Ru(I)−$3O_{ad}O_{sub}$ (≡Ru(I)−4O). In fact, the sinking of O from the top to the subsurface layer will leave a vacancy, and thus the Ru(I)−$2O_{ad}O_{sub}$ is very likely. As can be expected the shift of the Ru(II) component induced by the incorporated oxygen leaves only the "bulk" component at "zero" energy position, which accounts for the apparently reduced weight at this energy.

At this stage we again observed small differences in the line shape of the Ru $3d_{5/2}$ spectra from different spots, due to certain variations in the intensity of the different components. The TD spectrum of this stage is dominated by the α-peak, and the corresponding O amount is ~1.5 ML. The β-peak, emerging at 920 K originates from some oxygen incorporated below the second layer via a surface-defect mediated channel.[14] The LEED pattern of this surface still shows the (1 × 1) spots, but with an increased background intensity.

High oxygen exposure of 10^{12} mbar·s caused very significant changes in the relative weight of the components, as manifested by the bottom Ru $3d_{5/2}$ spectrum. According to the O_2 TD spectra the amount of accumulated oxygen is ~3 ML.[11,12,14] This rather broad and shapeless spectrum has a substantially reduced "bulk" component, indicative for formation of O-rich thin film of thickness of ~4−5 Å. The LEED pattern showed weak and diffuse (1 × 1) spots on an intense background, indicating that the incorporation of 2 ML of oxygen has not only deformed the lattice,[1] but has also disturbed the long-range order of the topmost layer. Since a disordered O-rich state supposes coexistence of different Ru−O bonding configurations, to account for that we allowed broadening and small energy variations of the Ru(I)−4O and Ru(II)−O components.

B. Oxidation of a Defect-Rich Ru(0001) Surface. The results in Figure 3 evidence the correlation between the surface "roughness" and the amount of accumulated oxygen. Here the sample surface is intentionally disordered by a gentle Ar^+ sputtering procedure (500 eV, 1.7 μA, 120 s). This introduces many monoatomic Ru vacancies randomly distributed over the two topmost layers,[14] reflected by the significant reduction of the surface component Ru(I) in the Ru $3d_{5/2}$ spectra (not shown). The Ru $3d_{5/2}$ spectra measured after three different LT oxygen exposures are deconvoluted by using the same components, as in Figure 2, allowing broadening and small variations in the energy positions. The major differences in the spectral evolution of the defected surface can be summarized as follows. The bulk component loses intensity faster, reflecting the enhanced incorporation rate of oxygen via a defect-mediated channel.[14] The disorder of the surface affects mostly the weight of the Ru(I)−4O component at 1.4 eV, which is very weak in all three spectra. The shape and energy position of the broad and featureless Ru $3d_{5/2}$ spectrum corresponding to the highest oxygen load of ~4 ML is clearly different from the spectrum of the RuO_2 phase formed under HT conditions (see Figure 1), and no "oxide" satellite appeared even in the spectra with the highest oxygen load. This confirms that at $T < 500$ K the formation of an ordered oxide phase cannot be completed even starting with a defect-rich surface. In fact, the spectrum with

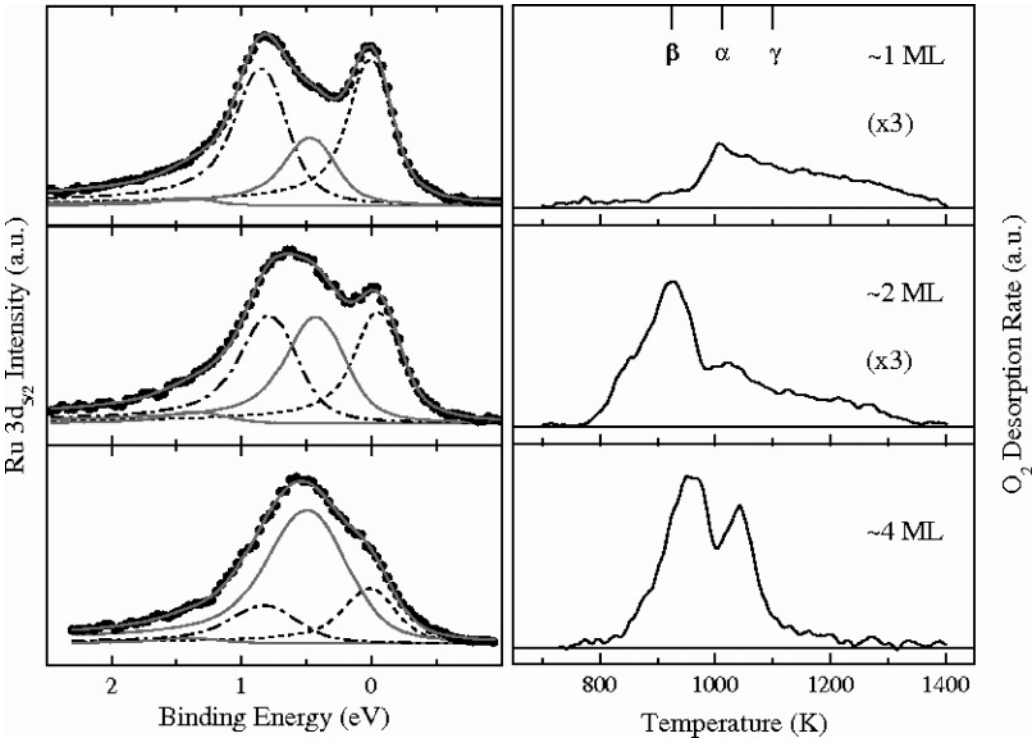

Figure 3. Left panel: Ru $3d_{5/2}$ spectra taken after different exposures of a "defect" Ru(0001) surface at 475 K to 10^5 (~1 ML), 10^8 (~2 ML), and 10^{12} mbar s (~4 ML). The deconvolution is performed with use of the components shown in Table 1. The dotted line is the Ru $3d_{5/2}$ bulk component. Right panel: The TD spectra, which quantify the oxygen content of the corresponding Ru $3d_{5/2}$ spectra in the left panel to 1, ~2, and ~4 ML, respectively.

the highest oxygen load of ~4 ML in Figure 3 strongly resembles the spectrum of the bright regions formed in the advanced HT oxidation, displayed in Figure 1b. The dominant component in both spectra is at ~0.4−0.45 eV, assigned above to the amorphous few layers thick Ru_xO_y film. Thus the HT disordered phase, coexisting with well-developed RuO_2 islands, is comparable with the disordered LT phase with the highest oxygen load. Further proof that even starting from a disordered surface the formation of a RuO_2 phase is kinetically hindered below 500 K is the O_2 TD spectrum, which does not contain a γ peak at 1100 K, the characteristic desorption feature of RuO_2.[11] The dominant TD feature is the β-peak, which apparently represents also the desorption from the amorphous Ru_xO_y state.

C. Temperature-Induced Reorganization of the Saturated LT Oxidation State. The "oxygen-saturated" ~3 ML LT state formed at 475 K, starting from the well-ordered Ru(0001) surface, loses oxygen upon annealing at higher temperatures, as illustrated by the Ru $3d_{5/2}$ spectra in Figure 4. The gradual increase of the bulk component before the onset of desorption (~800 K) reflects a loss of oxygen via temperature-assisted penetration below the second layer. In the temperature range 500−750 K the Ru(I)−4O component at 1.4 eV gradually decreases until complete extinction, accompanied by attenuation of the Ru(II)−O component and a gradual shift of the Ru(I)−4O* component toward the energy position of the Ru(I)−3O adsorption component. This temperature-induced process can be simply described by the following scheme: O_{ad}−Ru(I)−$O(sub)_{x>1}$−Ru(II) → O_{ad}−Ru(I)−$O(sub)_{x<1}$−Ru(II), where a fraction of O_{sub} penetrates below the second Ru layer. Here x accounts for the monolayers of O atoms incorporated between the first and second layer. At higher temperatures, 820 and 870 K, when the oxygen desorption starts the components of the oxygen adsorption phases, Ru(I)−3O and Ru(I)−2O (see Table 1), replace the Ru(I)−4O* and Ru(II)−O components, respectively.

4. Discussion

The evolution of the Ru $3d_{5/2}$ spectra indicates that the growth of RuO_2(110) is kinetically hindered under LT oxidation conditions of Ru(0001), i.e., the incorporation of O atoms is limited to the top 2−3 Ru layers forming an amorphous O-rich film. Here, we will focus on the results obtained for the ordered Ru(0001) surface, more relevant to the theoretical predictions. The Ru $3d_{5/2}$ spectrum of the most heavily oxygen-loaded Ru (~3 ML in Figure 2) shows the coexistence of at least three Ru−O bonding configurations. In the frame of the theoretical calculations[1,2] the 3 ML of oxygen should be accommodated on the surface and between the first and second layer, as a trilayer surface oxide, floating on the O-covered second Ru layer, i.e., O_{ad}−Ru(I)−O_{sub}···O_{ad}−Ru(II). This is accompanied by an expansion of the lattice so that the top O−Ru−O trilayer is almost decoupled from the underlying Ru metal and the electronic and geometric structure of the second Ru layer resembles an O−(1 × 1) covered Ru(0001).[21]

In the frame of this scenario, the growth and evolution of the Ru(II)−O and the two Ru(I)−4O components can be ascribed to sequential occupation of the interstitial sites.[1] An O adatom sinking from the hcp or fcc site to a tetra-I or octahedral site binds to the Ru(II) atoms below and affects the Ru(I) atoms already bound to 3 O adatoms. As suggested above, the two Ru(I)−4O components account for the subsurface O in the tetra-I or octahedral site. Since the oxygen incorporation also gradually deforms the surface lattice, one cannot exclude several on-surface/subsurface site organizations, including displacement of the adsorbed oxygen from hcp to fcc sites. Tentatively we can ascribe the Ru(I)−4O components to the trilayer surface oxide, O_{ad}−Ru(I)−O_{sub}. The simultaneous appearance and growth of the Ru(II)−O component support this assignment. After incorporation of ~1 ML of O between the first and the second Ru layer the additional oxygen should either penetrate

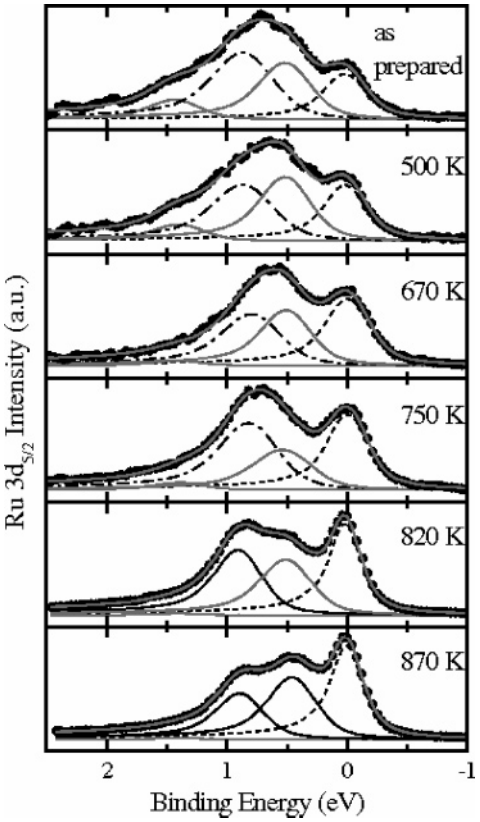

Figure 4. Evolution of the Ru $3d_{5/2}$ spectrum of an "oxygen-saturated" Ru(0001) surface (~3 ML) during stepwise annealing to different temperatures. The deconvolution is performed with use of the components shown in Table 1. The dotted line is the Ru $3d_{5/2}$ bulk component.

between the second and third layer or, as predicted by the DFT calculation,[1,2] will continue to reside between the first and second layer. Apparently, at total coverage >2 ML the additional oxygen leads to the transition from $O_{ad}-Ru(I)-O_{sub}-Ru(II)$ to $O_{ad}-Ru(I)-O_{sub}\cdots O_{sub}-Ru(II)$ state. The accommodation of more than 1 ML subsurface oxygen, yielding a trilayer surface oxide, requires significant lattice expansion and introduces a disorder. This is reflected by the broadening of the Ru(II)−O and Ru(I)−4O components, probably due to coexistence of poorly defined multiple Ru−O coordinations.

5. Concluding Remarks

Combining XPS microscopy and TDS we demonstrate that the formation of a crystalline rutile RuO_2 phase starting from an ordered Ru(0001) surface is kinetically hindered at temperatures lower than 500 K. The main reason is the limited incorporation of oxygen, which does not reach the critical coverage of 4 ML (two rutile layers). This suggests that the potential energy surface that governs the transport of oxygen from the surface to the bulk has an energy barrier for penetration below the second layer, which can be overcome only at higher temperatures. The LT intermediate states, identified in the present study, describe well the formation of the surface oxide and provide spectroscopic evidence for subsurface oxygen, occupying different sites between the first and second layer. The results show that the Ru surface oxide is unstable and should have a very short lifetime during HT oxidation. The LT oxidation of a disordered surface leads to a more advanced oxidation state. The spectroscopic features of this state indicate the presence of unsaturated oxide-like Ru configurations. This

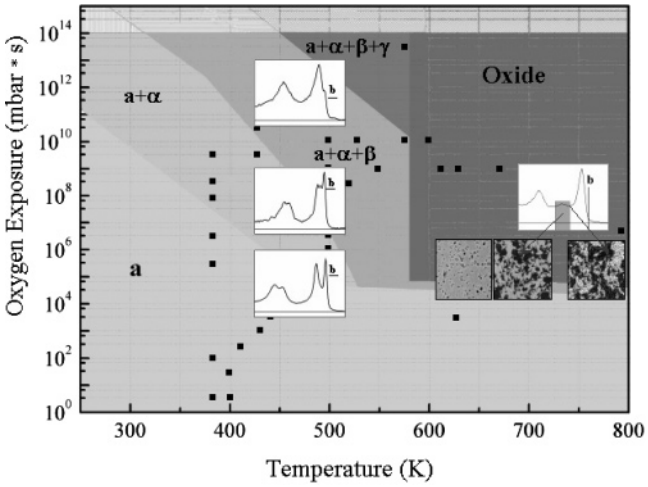

Figure 5. Diagram of the Ru oxidation state as a function of the O_2 exposure (in mbar s) and temperature. The patterned areas are determined on the basis of a large set of O_2-TD spectra. (a), α, *β*, and *γ* are the peaks appearing in the O_2 TD spectra, which correspond to the adsorption phases (a), the different subsurface phases (α, *β*), and the onset of oxidation (*γ*). The black squares indicate the (exposure-*T*) space, where the system is characterized by XPS spectroscopy and/or spectromicroscopy. The typical Ru 3d spectra of the LT phase with 1, 2, and 3 ML of oxygen and of the oxide phase are plotted as well. Here, b marks the Ru $3d_{5/2}$ bulk peak. For the oxide phases, obtained at three different temperatures, the three images and a typical oxide spectrum illustrate the anisotropic growth of the RuO_2.

advanced LT oxidation state is similar to the amorphous few layers thick Ru_xO_y precursor, coexisting with the rutile RuO_2 islands during HT oxidation. Combining the present results with those previously obtained under varying HT reaction conditions,[12] we propose the diagram in Figure 5, which summarizes the different intermediate states involved in the oxidation of the Ru(0001) surface. It suggests that, depending on the temperature, exposure time, and partial pressure of the reactants, the active phase during catalytic oxidation reactions may not only be the rutile RuO_2 phase, but also the amorphous O-rich state with incorporated oxygen.

Acknowledgment. R.B. and H.N. acknowledge the financial support by the DFG through project Ni-452. L.A. acknowledges financial support by EC Marie Curie Fellowship. The EU is acknowledged for financial support under Contract No. NMP3-CT-2003-505670 (NANO2) and I3 project IA-SFS.

References and Notes

(1) Todorova, M.; Li, W. X.; Ganduglia-Pirovano, M. V.; Stampfl, C.; Reuter, K.; Scheffler, M. *Phys. Rev. Lett.* **2002**, *89*, 96103.
(2) Reuter, K.; Stampfl, C.; Ganduglia-Pirovano, M. V.; Scheffler, M. *Chem. Phys. Lett.* **2002**, *352*, 311.
(3) Böttcher, A.; Niehus, H.; Schwegmann, S.; Over, H.; Ertl, G. *J. Phys. Chem. B* **1997**, *101*, 11185.
(4) Over, H.; Kim, Y. D.; Seitsonen, A. P.; Lundgren, E.; Schmid, M.; Varga, P.; Morgante, A.; Ertl, G. *Science* **2000**, *287*, 1474.
(5) Over, H.; Seitsonen, A. P.; Lundgren, E.; Schmid, M.; Varga, P. *Surf. Sci.* **2002**, *515*, 143.
(6) Madhavaram, H.; Idriss, H.; Wendt, S.; Kim, Y. D.; Knapp, M.; Over, H.; Assmann, J.; Löffler, V.; Muhler, M. *J. Catal.* **2001**, *202*, 296.
(7) Over, H.; Muhler, M. *Prog. Surf. Sci.* **2003**, *72*, 3.
(8) Böttcher, A.; Niehus, H. *J. Chem. Phys.* **1999**, *110*, 3186.
(9) Böttcher, A.; Conrad, H.; Niehus, H. *J. Chem. Phys.* **2000**, *112*, 4779.
(10) Böttcher, A.; Krenzer, B.; Conrad, H.; Niehus, H. *Surf. Sci.* **2002**, *504*, 42.
(11) Blume, R.; Niehus, H.; Conrad, H.; Böttcher, A. *J. Chem. Phys.* **2004**, *204*, 3871.
(12) Böttcher, A.; Starke, U.; Conrad, H.; Blume, R.; Gregoratti, L.; Kaulich, B.; Barinov, A.; Kiskinova, M. *J. Chem. Phys.* **2002**, *117*, 8104.

(13) Over, H.; Seitsonen, A. P.; Lundgren, E.; Wiklund, M.; Andersen, J. N. *Chem. Phys. Lett.* **2001**, *342*, 467.
(14) Blume, R.; Niehus, H.; Conrad, H.; Böttcher, *J. Phys. Chem. B* **2004**, *108*, 14332.
(15) Kiskinova, M.; Marsi, M.; Di Fabrizio, M.; Gentili, M. *Surf. Rev. Lett.* **1999**, *6*, 265; http://www.elettra.trieste.it/experiments/beamlines/esca/index.html.
(16) Seah, M. P.; Dench, W. A. *Surf. Interface Anal.* **1979**, *1*, 2.
(17) Madey, T. E.; Engelhardt, H. A.; Menzel, D. *Surf. Sci.* **1975**, *48*, 304.
(18) Stampfl, C.; Schwegmann, S.; Over, H.; Scheffler, M.; Ertl, G. *Phys. Rev. Lett.* **1996**, *77*, 3371.
(19) Lizzit, S.; Baraldi, A.; Groso, A.; Reuter, K.; Ganduglia-Pirovano, M. V.; Stampfl, C.; Scheffler, M.; Stichler, M.; Keller, C.; Wurth, W.; Menzel, D. *Phys. Rev. B* **2001**, *63*, 205419.
(20) Reuter, K.; Scheffler, M. *Surf. Sci.* **2001**, *490*, 20.
(21) Reuter, K.; Stampfl, C.; Ganduglia-Pirovano, M. V.; Scheffler, M. *Phys. Rev. B* **2002**, *65*, 165403.
(22) Kostov, K. L.; Gsell, M.; Jakob, P.; Moritz, T.; Widdra, T.; Menzel, D. *Surf. Sci.* **1997**, *394*, L138.
(23) Baraldi, A.; Lizzit, S.; Comelli, G.; Kiskinova, M.; Rosei, R.; Honkala, K.; Norskov, K. *Phys. Rev. Lett.* **2004**, *93*, 46101 and the references therein.
(24) Baraldi, A.; Lizzit, S.; Paolucci, G. *Surf. Sci.* **2000**, *457*, L354.